Ebola Virus VP35 Hijacks PKA-CREB1 Pathway for Replication and Pathogenesis by AKIP1 Association

Cheng Cao (caoc@nic.bmi.ac.cn)
Beijing Institute of Biotechnology
Lin Zhu
Beijing Institute of Biotechnology
Ting Gao
Beijing Institute of Biotechnology
Xuan Liu
Beijing Institute of Biotechnology https://orcid.org/0000-0001-6369-9259

Biological Sciences - Article

Keywords: Ebola Hemorrhagic Fever, Viral RNA-dependent RNA Polymerase, A Kinase Interfacing Protein, Viral Inclusion Bodies, Coagulation-related Genes

Posted Date: January 25th, 2021

DOI: https://doi.org/10.21203/rs.3.rs-138642/v1

Abstract

Ebola virus (EBOV), one of the deadliest viruses, is the cause of fatal Ebola hemorrhagic fever (EHF)[1,2]. The underlying mechanism of viral replication and EBOV-related hemorrhage is not fully understood. Here, we show that EBOV VP35, a cofactor of viral RNA-dependent RNA polymerase, binds human A kinase interacting protein (AKIP1), which consequently activates protein kinase A (PKA) and PKA-downstream transcription factor CREB1. During EBOV infection, CREB1 is recruited into EBOV ribonucleoprotein complexes in viral inclusion bodies (VIBs) and employed for viral replication. AKIP1 depletion or PKA-CREB1 inhibition dramatically impairs EBOV replication. Meanwhile, the transcription of several coagulation-related genes, including *THBD* and *SERPINB2*, is substantially upregulated by VP35-dependent CREB1 activation, which may contribute to EBOV-related hemorrhage. The finding that EBOV VP35 hijacks the host PKA-CREB1 signal axis for viral replication and pathogenesis provides novel potential therapeutic approaches against Ebola virus disease.

Main Text

Ebola virus disease (EVD), also known as EHF, is the deadliest infectious disease caused by EBOV infection[1]. The largest EVD epidemic during 2013-2016 caused more than 28,000 confirmed cases and more than 11,000 deaths[2]. The second largest outbreak beginning in 2018 resulted in 3470 infections and 2287 deaths (https://www.who.int/csr/don/26-June-2020-ebola-drc/en/). As the pathogens causing EVD, the *Ebolavirus* genus contains five species, including *Zaire ebolavirus* (also known as EBOV), *Sudan ebolavirus* (SUDV), *Bundibugyo ebolavirus* (BDBV), *Tai Forest ebolavirus* (TAFV) and *Reston ebolavirus* (RESTV, nonpathogenic in humans)[3], of which *Zaire ebolavirus* is the most virulent, with a fatality rate as high as 90%, and is the major cause of EVD outbreak[2,4].

Ebola virus is an enveloped, nonsegmented negative-sense (NNS) RNA virus[5]. The 19 kb viral genome comprises seven genes encoding nucleoprotein (NP), virion protein 35 (VP35), VP40, glycoprotein (GP), VP30, VP24 and large protein (L) sequentially[1]. NP, VP35, VP30 and L are associated with the viral RNA genome, forming the nucleocapsid termed the viral ribonucleoprotein complex (RNPs)[5]. VIBs formed in EBOV-infected cells are specialized intracellular compartments serving as sites for EBOV replication and the generation of progeny viral RNPs[6,7]. In VIBs, the EBOV genome is replicated and transcribed by viral polymerase complexes[8]. Among RNPs, VP35 serves as a cofactor of RNA-dependent RNA polymerase (RdRp) and contributes to viral replication by homo-oligomerization through a coiled-coil domain[9], as well as the NTPase and helicase-like activities revealed recently[10]. Several host proteins, such as dynein light chain (LC8), DRBP76, PACT, TRIM6, and Staufen1, are moderately dedicated to viral replication by VP35 association[11-15]. In addition, VP35 is also involved in host innate immune antagonism by inhibiting type I interferon (IFN) production, suppressing RNA silencing and inhibiting dendritic cell maturation[16-18].

Protein kinase A (PKA) is a well-known sensor of the second messenger cyclic AMP (cAMP), playing fundamental roles in a variety of biological processes. Upon activation, PKA phosphorylates numerous

substrates in the cytoplasm and nucleus, including cAMP-responsive element binding protein 1 (CREB1). PKA-mediated CREB1 S133 phosphorylation activates the transcription of downstream genes in response to hormonal stimulation in a cAMP-dependent manner. PKA is also involved in hepatitis C virus entry, Zika virus infection, and organelle transport regulation in response to adenovirus infection[19-21]. However, the potential role of PKA in EBOV infection and pathogenesis is still unknown.

A kinase interacting protein 1 (AKIP1) is a PKA-interacting protein that binds to the amino terminus of the protein kinase A catalytic subunit alpha (PRKACA) and potentiates the translocation of PRKACA into the nucleus[22]. In this study, we found that EBOV VP35 significantly potentiates the activation of the PKA-CREB1 signaling pathway by AKIP1 association, thereby facilitating viral replication and resulting in a disordered expression of coagulation-related genes. The crucial roles of the AKIP1-PKA-CREB1 signaling axis in viral replication and pathogenesis may direct the development of antiviral and anti-coagulopathy therapy of EVD.

EBOV VP35 is associated with host AKIP1 and thereby activates PKA

Yeast two-hybrid screening using EBOV VP35 as bait against the human liver cDNA library suggested that human AKIP1 was a candidate for VP35 association (Extended Data Fig. 1a). To substantiate their interaction in the EBOV targeting hepatic cells, HepG2 cells derived from human liver were transfected with Flag-VP35 or Flag-vector as a control and subjected to anti-Flag immunoprecipitation and immunoblotting with the indicated antibodies. The presence of endogenous AKIP1 in the Flag-VP35, but not the Flag-vector, immunoprecipitates suggested the association of VP35 with AKIP1 (Fig. 1a). The associations of VP35 and AKIP1 carrying reciprocal tags were also observed in HEK293 cells (Extended Data Fig. 1b, c). Then, the crucial sequence of VP35 responsible for AKIP1 association was determined by VP35 truncation and mutation (Extended Data Fig. 1d). We found that the C-terminus of VP35 (199-340 amino acids, VP35C) was required for the VP35-AKIP1 interaction (Extended Data Fig. 1e). Notably, triple alanine replacements of F239/K319/R322, which play a essential role in dsRNA binding and inhibiting host type I IFN responses[11,23], resulted in the abrogation of the VP35-AKIP1 association (Fig. 1b and Extended Data Fig. 1d). Nevertheless, the association of VP35 and AKIP1 could be observed without the presence of viral dsRNA (Fig. 1a). For AKIP1, the C-terminal region (101-210 amino acids), but not the N-terminal region (1-100 amino acids), was involved in VP35 association (Fig. 1c and Extended Data Fig. 1d).

To further illustrate their association *in situ* in the cells, the colocalization of exogenously expressed GFP-VP35 with Myc-AKIP1 was detected in the HeLa cells (Extended Data Fig. 2a). In concert, viral VP35 was nearly completely colocalized with endogenous AKIP1 in HepG2 cells infected with live EBOV (Fig. 1d). Further, an *in situ* Duolink proximity ligation assay (PLA) was performed to detect VP35:AKIP1 complexes. Cytoplasmic complexes (the red signals) of endogenous AKIP1 with GFP-VP35 (Extended

Data Fig. 2b) but not GFP (Extended Data Fig. 2c) was observed in HepG2 cells. Accordingly, the obvious viral VP35:AKIP1 complexes were also observed in the HepG2 cells infected with EBOV, or replication and transcription-competent virus-like particles (trVLPs) of EBOV which can simulate EBOV infection[24] (Fig. 1e). As control, no PLA signals were observed in non-infected cells (Extended Data Fig. 2d). These results collectively demonstrated that EBOV VP35 interacts with AKIP1 in host cells, most likely in the viral inclusion bodies (VIBs) (Extended Data Fig. 3).

As an activator of PRKACA, AKIP1 demonstrated a significantly enhanced PRKACA binding capability in the presence of VP35 (Fig. 1f), which was also confirmed by *in situ* PLA in GFP-VP35-expressing cells compared to the control cells (Extended Data Fig. 4a). Moreover, GFP-VP35 (but not GPP) expression potentiates nuclear translocation of PRKACA in wildtype (WT) but not *AKIP1*$^{-/-}$ HepG2 cells (Fig. 1g and Extended Data Fig. 4b, c), which may exclude the direct activation of PRKACA by viral VP35. Consequently, VP35-transfected HepG2 cells showed considerably increased PKA substrate phosphorylation than that of control by anti-pPKA-substrates immunoblotting (Fig. 1h). Further, as determined by an *in vitro* non-radioactive PKA kinase assay, VP35 expression potentiated PKA activity in WT (~2.6 fold) but not AKIP1-depleted HepG2 cells (Fig. 1i). These data collectively suggested that VP35-induced PKA activation is dependent on AKIP1 association.

EBOV VP35 promotes PKA-mediated CREB1 phosphorylation

We next assessed the effect of VP35 on the activation of CREB1, a well-defined PKA downstream substrate. CREB1 S133 phosphorylation was significantly potentiated by Ad-VP35 expression, which could be further promoted by FSK, an activator of PRKACA, and suppressed by H89, an inhibitor of PRKACA (Fig. 2a). Moreover, the nuclear accumulation of phosphorylated CREB1 was also induced by Ad-VP35 expression, as well as EBOV or trVLPs infection (Fig. 2b, c). In agreement with PKA activation, VP35 failed to potentiate CREB1 phosphorylation in AKIP1 knockdown (Fig. 2d), or AKIP1-depleted cells (Fig. 2e), suggesting that viral VP35 potentiates CREB1 phosphorylation through AKIP1. Notably, a significantly increased CREB1 S133 phosphorylation was observed in the lung and liver tissues of Ad-VP35 but not Ad-null infected mice (Fig. 2f, Extended Data Fig. 4d). These results collectively demonstrated that EBOV VP35 promotes CREB1 phosphorylation *in vitro* and *in vivo* in an AKIP1-dependent manner.

EBOV VP35 hijacks CREB1 into the replication complexes in VIBs

In addition to facilitating the nuclear accumulation of phosphorylated CREB1, to our surprise, a substantial proportion of phosphorylated CREB1 was observed to be colocalized with NP and VP35 in VIB-like compartments in the cytoplasm when the cells were infected with EBOV or trVLPs (Fig. 2c and Extended Data Fig. 5a). In support of this observation, CREB1 was further demonstrated to be recruited

into the viral replication compartments and colocalized with both viral VP35 (Fig. 3a, b) and NP (Extended Data Fig. 5b) after EBOV trVLPs infection. However, this colocalization could be abrogated by the CREB1 inhibitor 666-15, as well as AKIP1 depletion, resulting in a substantial decrease in the amount and size of VIBs (Fig. 3a, b and Extended Data Fig. 5b). In agreement with this observation, CREB1 recruitment into VIBs was similarly detected in cells infected with live EBOV (Fig. 3c). These finding suggested that the presence of AKIP1 as well as PKA-CREB1activation is indispensable for CREB1 recruitment into VIBs.

To further explore the colocalization of CREB1 with VIBs, lysates of HepG2 cells infected with EBOV trVLPs were fractioned using sucrose density gradient centrifugation, and CREB1 was enriched in the 7th and 8th fractions along with viral VP35 and NP (Fig. 3d). Accordingly, VP35, NP, and viral RNA polymerase L were all present in anti-CREB1 immunoprecipitates prepared from the combined 7th and 8th fractions (Fig. 3e). Moreover, in EBOV trVLPs-infected HepG2 cells, an RNA-IP assay with an anti-CREB1 antibody showed that, in the presence of AKIP1, CREB1 was more strongly associated with the 3' leader region of the viral RNA genome containing essential signals required for RNA synthesis[15] but not the 5' trailer region (Fig. 3f). These results cumulatively demonstrated that CREB1 is recruited into viral RNP complexes by VP35, which may contribute to viral replication.

Active CREB1 is indispensable for EBOV replication

We then investigated whether AKIP1-dependent CREB1 recruitment would impact EBOV replication using a modified trVLPs carrying a luciferase reporter (Luc-trVLPs). Compared with wild-type cells, AKIP1 depletion resulted in up to a 1,300-fold inhibition of Luc-trVLPs replication in two independent cell clones, as indicated by luciferase activity (Fig. 4a, right), viral genome RNA (vRNA) determination (Fig. 4b), and immunostaining (Extended Data Fig. 6a). AKIP1 knockdown also resulted in a significant inhibition of viral replication to a lesser extent (Extended Data Fig. 6b). As a result of the VP35-AKIP1 association, PKA activation evidently participated in viral replication by the observation that Luc-trVLPs replication was considerably inhibited ~7-fold in p1 and ~15-fold in p2 by the PKA inhibitor H89, while it was potentiated ~1.7-fold by the PKA activator FSK (Fig. 4c). Furthermore, a much more powerful antiviral effect was observed when the cells were treated with the CREB1 inhibitors KG-501 (~1,100-fold in p1) and 666-15 (~6,800-fold in p1) (Fig. 4d). The 50% inhibitory concentration (IC50) of 666-15 was as low as ~50 nM, which was far less than the IC50 of T705 (6 mM), a broad-spectrum antiviral candidate that had been clinically used in EVD patients in Sierra Leone[25] (Fig. 4e). In agreement, live EBOV replication was also dramatically inhibited by AKIP1 depletion (~85-fold), H89 (~19-fold at 10 μM) or 666-15 (~150-fold at 1 μM), as assayed by qRT-PCR of vRNA (Fig. 4f) or immunostaining (Extended Data Fig. 6c) on the 4^{th} day post infection (d.p.i.). Amount of Ebola virus released into the medium were also significantly inhibited by 666-15 (~12-fold at 4 d.p.i.) as tittered by median tissue culture infective dose ($TCID_{50}$) (Fig. 4g). These results collectively demonstrated that the AKIP1-PKA-CREB1 axis plays crucial roles in EBOV replication.

EBOV VP35 modulates the transcription of CREB1-regulated coagulation-related genes

In concert with the findings that VP35-induces CREB1 phosphorylation and nuclear translocation, CREB1 directed transcription was significantly promoted by VP35 expression, and further by PKA activation, in the luciferase reporter system harboring the CREB1-binding element (Fig. 5a). Then, transcriptome in HepG2 cells transfected with Flag-VP35 or Flag vector was investigated by microarray[26]. Differentially expressed gene (DEG) were analyzed (Extended Data Fig. 7a), and a panel of coagulation-related genes were found significantly enriched (Extended Data Fig. 7b, c), including *THBD*, a biomarker of EBOV-induced hemorrhage and death[27], and *SERPRINB2*, a potent inhibitor of urokinase-type plasminogen activator, thrombin and other proteases[28]. The mRNA levels were further quantified by reverse transcription qRT-PCR. In line with the results, the mRNA level of both *THBD* and *SERPINB2* was significantly upregulated by VP35 in HUVECs (Fig. 5b) and HepG2 (Extended Data Fig. 7d) cells, which could be nearly abolished by the PKA inhibitor (Fig. 5b and Extended Data Fig. 7d). Accordingly, protein level of thrombomodulin (TM, *THBD* encoding protein) and SerpinB2 was upregulated by VP35 expression (Extended Data Fig. 7e, f). In agreement, live EBOV infection resulted in a significant upregulation of *THBD* and *SERPINB2* transcription, which was compromised by H89 or 666-15 treatment, as well as AKIP1 depletion (Fig. 5c). These results collectively indicate that VP35 may cause coagulation disorder by modifying TM and SerpinB2 expression through the AKIP1-PKA-CREB1 signal axis.

Furthermore, because no laboratory was permitted to work with animal infection of EBOV in China, Ad-VP35 was employed to assess the effect of EBOV VP35 protein on coagulation. As expect, TM levels were significantly increased in WT mice but not in *Akip1*$^{-/-}$ littermates by Ad-VP35 (not by Ad-null) infection (Fig. 5d and Extended Data Fig. 7g). Ad-VP35 infection also resulted in a prolonged prothrombin time (PT), a reduced fibrinogen (FIB) level, and consequently a prolonged tail bleeding time in the WT but not *Akip1*$^{-/-}$ mice exposed to Ad-VP35, regardless challenged with or without LPS, a well-known activator of coagulation[29], which could be nearly completely rescued by the CREB1 inhibitor 666-15 (Fig. 5e, Extended Data Fig. 7h). In agreement with these findings, Ad-VP35 infected WT mice exhibited significantly higher mortality than *Akip1* null mice (77.8% vs 11.1%) when challenged with LPS (Fig. 5f and Extended Data Fig. 7g), and the VP35 potentiated mortality of infected WT mice could be completely rescued by CREB1 inhibitor 666-15 (Fig. 5f). Taken together, these results demonstrated that VP35 causes coagulation disorder in mice through the AKIP1-PKA-CREB1 pathway. Although other pathways regulated by CREB1 could not be excluded, VP35 induced coagulation disorder may play an important role in LPS-mediated mice mortality.

Discussion

Accumulated studies of EBOV pathogenesis have revealed a panel of human cellular proteins that participate or regulate viral replication by interacting with viral proteins[12,30-32] or cis elements in the viral genome[15]. In this study, we found that the cAMP-responsive transcription factor CREB1 is hijacked into viral replication complexes by EBOV VP35. This process is dependent on the interaction between viral

VP35 and host AKIP1, which activates PKA and eventually results in CREB1 phosphorylation and activation. Live EBOV or trVLPs infection resulted in an obvious accumulation of CREB1 in VIBs coexisting with VP35, NP, L and 3' of viral genomic RNA, which is essential for viral RNA replication (Fig. 3a, c, e, f), suggesting that EBOV hijacks the transcription factor CREB1 for viral gene transcription and replication. CREB1 promotes mRNA synthesis in cells by interacting with RNA polymerase II through glutamine-rich domain (Q2)[33] and TBP associated factor 4 (TAF4)[34]. However, the exact mechanism by which CREB1 potentiates viral RNA-dependent RNA polymerase in viral replication remains to be investigated.

The pathogenesis of lethal hemorrhage caused by EBOV has not been well understood until now. The secreted glycoprotein (sGP) of EBOV is considered to be a virulence factor responsible for vascular dysregulation and hemorrhage by inducing endothelial modifications and lymphocyte adhesion, thereby destroying the barrier function of endothelial cells[35]. However, a recent study also suggested that sGP may not play a key role with respect to vascular dysregulation during EBOV infection[36]. Here, we showed that viral VP35-mediated PKA activation resulted in the phosphorylation of a number of PKA substrates, such as CREB1 presented in this work, and vasodilator-stimulated phosphoprotein (VASP) (Extended Data Fig. 8), a well-defined PKA substrate involved in platelet activation and aggregation[37]. Importantly, EBOV infection resulted in the overexpression of *THBD* (encoding TM) and *SERPINB2* (Fig. 5c). TM is ubiquitously expressed on the vascular endothelium, binds to thrombin, forming the TM-thrombin complex and acts as an anticoagulant. In addition, the thrombin-TM complex activates protein C to produce APC, which inactivates coagulation factors (F) Va and VIIIa in the presence of protein S, thereby inhibiting further thrombin formation[38]. The TM/APC system is considered a guardian of blood coagulation and vascular integrity[38]. Sustained overexpression of TM can result in the exhaustion of thrombin. In fact, TM levels were significantly elevated and considered to be a biomarker of death and hemorrhage in EVD patients[27]. SerpinB2, as an inhibitor of urokinase-type plasminogen activator, is commonly considered as an inhibitor of fibrinolysis. However, recent work by Schroder *et al*. demonstrated that mice with *SERPINB2* deficiency showed significant reductions in tail bleeding times by dysregulated platelet activation[28]. In accordance with *THBD* and *SERPINB2* upregulation, Ad-VP35-infected mice demonstrated a prolonged tail bleeding time (Fig. 5e), prothrombin time (PT) and a reduced FIB level (Extended Data Fig. 7h). Mice infected with a mouse-adapted strain of EBOV (MA-EBOV) also showed a prolonged thrombin time (TT), PT, and activated partial thromboplastin time (aPTT) as well as decreased FIB levels[39]. Our findings reveal the potential mechanisms of disordered coagulation and extensive microvascular thrombosis induced by viral VP35.

The finding that the AKIP1-PKA-CREB1 signaling axis is hijacked by VP35 and employed for EBOV replication and virus-induced coagulopathy provides new potential targets for the therapy of EBOV-related disease (Extended Data Fig 9). 666-15, a small molecular CREB1 inhibitor with an IC50 value of ~67 nM and well tolerated by mice with acceptable pharmacokinetics[40,41], showed promising efficacy in suppressing viral replication (up to 6,800-fold) and viral-induced overexpression of TM and SerpinB2. Similar inhibitory efficacy was also observed with the PKA inhibitor H89, although to a lesser extent.

Notably, AKIP1 depletion or CREB1 suppression showed a less effect on live EBOV proliferation than trVLPs (Fig. 4). Down-regulated VP35 level by AKIP1 expression (Fig. 2e) may compromise the effect of VP35-induced AKIP1-PKA-CREB1 activation and function as a negative feedback. A more powerful inhibition of AKIP1 depletion or CREB1 suppression on trVLPs replication may be explained by the redundant exogenous VP35 supply in the system. In summary, our findings provide a novel approach for the development of therapeutics against EVD.

References

1 Mahanty, S. & Bray, M. Pathogenesis of filoviral haemorrhagic fevers. *Lancet Infect. Dis.* **4**, 487-498 (2004).

2 Rasmussen, A. L. Host Factors Involved in Ebola Virus Replication. *Curr. Top. Microbiol. Immunol.* **419**, 113-150 (2018).

3 Messaoudi, I., Amarasinghe, G. K. & Basler, C. F. Filovirus pathogenesis and immune evasion: insights from Ebola virus and Marburg virus. *Nat. Rev. Microbiol.* **13**, 663-676 (2015).

4 Jacob, S. T. *et al.* Ebola virus disease. *Nat. Rev. Dis. Primers* **6**, 13-43 (2020).

5 Feldmann, H., Jones, S., Klenk, H. D. & Schnittler, H. J. Ebola virus: from discovery to vaccine. *Nat. Rev. Immunol.* **3**, 677-685 (2003).

6 Hoenen, T. *et al.* Inclusion Bodies Are a Site of Ebolavirus Replication. *J. Virol.* **86**, 11779-11788 (2012).

7 Nanbo, A., Watanabe, S., Halfmann, P. & Kawaoka, Y. The spatio-temporal distribution dynamics of Ebola virus proteins and RNA in infected cells. *Sci. Rep.* **3**, 1206 (2013).

8 Misasi, J. & Sullivan, N. J. Camouflage and misdirection: the full-on assault of Ebola virus disease. *Cell* **159**, 477-486 (2014).

9 Reid, S. P., Cardenas, W. B. & Basler, C. F. Homo-oligomerization facilitates the interferon-antagonist activity of the ebolavirus VP35 protein. *Virology* **341**, 179-189 (2005).

10 Shu, T. *et al.* Ebola virus VP35 has novel NTPase and helicase-like activities. *Nucleic Acids Res.* **47**, 5837-5851 (2019).

11 Luthra, P. *et al.* Mutual antagonism between the Ebola virus VP35 protein and the RIG-I activator PACT determines infection outcome. *Cell host & microbe* **14**, 74-84 (2013).

12 Luthra, P., Jordan, D. S., Leung, D. W., Amarasinghe, G. K. & Basler, C. F. Ebola virus VP35 interaction with dynein LC8 regulates viral RNA synthesis. *J. Virol.* **89**, 5148-5153 (2015).

13 Bharaj, P. *et al.* The Host E3-Ubiquitin Ligase TRIM6 Ubiquitinates the Ebola Virus VP35 Protein and Promotes Virus Replication. *J. Virol.* **91**, e00833-17 (2017).

14 Shabman, R. S. *et al.* DRBP76 Associates With Ebola Virus VP35 and Suppresses Viral Polymerase Function. *J. Infect. Dis.* **204**, S911-S918 (2011).

15 Fang, J. *et al.* Staufen1 Interacts with Multiple Components of the Ebola Virus Ribonucleoprotein and Enhances Viral RNA Synthesis. *mBio* **9**, e01771-18 (2018).

16 Basler, C. F. *et al.* The Ebola virus VP35 protein functions as a type I IFN antagonist. *Proc. Natl. Acad. Sci. U. S. A.* **97**, 12289-12294 (2000).

17 Haasnoot, J. *et al.* The Ebola virus VP35 protein is a suppressor of RNA silencing. *Plos Pathog.* **3**, 794-803 (2007).

18 Yen, B., Mulder, L. C., Martinez, O. & Basler, C. F. Molecular basis for Ebolavirus VP35 suppression of human dendritic cell maturation. *J. Virol.* **88**, 12500-12510 (2014).

19 Farquhar, M. J. *et al.* Protein kinase A-dependent step(s) in hepatitis C virus entry and infectivity. *J. Virol.* **82**, 8797-8811 (2008).

20 Scherer, J., Yi, J. & Vallee, R. B. PKA-dependent dynein switching from lysosomes to adenovirus: a novel form of host-virus competition. *J. Cell Biol.* **205**, 163-177 (2014).

21 Cheng, F., Ramos da Silva, S., Huang, I. C., Jung, J. U. & Gao, S. J. Suppression of Zika Virus Infection and Replication in Endothelial Cells and Astrocytes by PKA Inhibitor PKI 14-22. *J. Virol.* **92**, e02019-17 (2018).

22 Sastri, M., Barraclough, D. M., Carmichael, P. T. & Taylor, S. S. A-kinase-interacting protein localizes protein kinase A in the nucleus. *Proc. Natl. Acad. Sci. U. S. A.* **102**, 349-354 (2005).

23 Leung, D. W. *et al.* Structural basis for dsRNA recognition and interferon antagonism by Ebola VP35. *Nat. Struct. Mol. Biol.* **17**, 165-172 (2010).

24 Hoenen, T., Watt, A., Mora, A. & Feldmann, H. Modeling the lifecycle of Ebola virus under biosafety level 2 conditions with virus-like particles containing tetracistronic minigenomes. *J. Vis. Exp.* **91**, e52381 (2014).

25 Bai, C.-Q. *et al.* Clinical and Virological Characteristics of Ebola Virus Disease Patients Treated With Favipiravir (T-705)—Sierra Leone, 2014. *Clin. Infect. Dis.* **63**, 1288-1294 (2016).

26 Li, D. *et al.* In Vitro and In Vivo Activities of Pterostilbene against Candida albicans Biofilms. *Antimicrob. Agents Chemother.* **58**, 2344-2355 (2014).

27 McElroy, A. K. *et al.* Ebola hemorrhagic Fever: novel biomarker correlates of clinical outcome. *J. Infect. Dis.* **210**, 558-566 (2014).

28 Schroder, W. A. *et al.* SerpinB2 deficiency in mice reduces bleeding times via dysregulated platelet activation. *Platelets* **30**, 658-663 (2018).

29 Yang, X. *et al.* Bacterial Endotoxin Activates the Coagulation Cascade through Gasdermin D-Dependent Phosphatidylserine Exposure. *Immunity* **51**, 983-996 (2019).

30 Batra, J. *et al.* Protein Interaction Mapping Identifies RBBP6 as a Negative Regulator of Ebola Virus Replication. *Cell* **175**, 1917-1930 (2018).

31 Iwasa, A. *et al.* Contribution of Sec61α to the Life Cycle of Ebola Virus. *J. Infect. Dis.* **204**, S919-S926 (2011).

32 Takahashi, K. *et al.* DNA Topoisomerase 1 Facilitates the Transcription and Replication of the Ebola Virus Genome. *J. Virol.* **87**, 8862-8869 (2013).

33 Mayr, B. & Montminy, M. Transcriptional regulation by the phosphorylation-dependent factor CREB. *Nat.Rev. Mol. Cell Biol.* **2**, 599-609 (2001).

34 Altarejos, J. Y. & Montminy, M. CREB and the CRTC co-activators: sensors for hormonal and metabolic signals. *Nat. Rev. Mol. Cell Biol.* **12**, 141-151 (2011).

35 Wahl-Jensen, V. M. *et al.* Effects of Ebola virus glycoproteins on endothelial cell activation and barrier function. *J. Virol.* **79**, 10442-10450 (2005).

36 de La Vega, M. A., Wong, G., Kobinger, G. P. & Qiu, X. The multiple roles of sGP in Ebola pathogenesis. *Viral Immunol.* **28**, 3-9 (2015).

37 Sudo, T., Ito, H. & Kimura, Y. Phosphorylation of the vasodilator-stimulated phosphoprotein (VASP) by the anti-platelet drug, cilostazol, in platelets. *Platelets* **14**, 381-390 (2003).

38 Ikezoe, T. Thrombomodulin/activated protein C system in septic disseminated intravascular coagulation. *J. Intensive Care* **3**, 1 (2015).

39 Rasmussen, A. L. *et al.* Host genetic diversity enables Ebola hemorrhagic fever pathogenesis and resistance. *Science* **346**, 987-991 (2014).

40 Xie, F. *et al.* Identification of a Potent Inhibitor of CREB-Mediated Gene Transcription with Efficacious in Vivo Anticancer Activity. *J. Med. Chem.* **58**, 5075-5087 (2015).

41 Li, B. X. *et al.* Systemic Inhibition of CREB is Well-tolerated in vivo. *Sci. Rep.* **6**, 34513 (2016).

Methods

Cell lines and transfections

HEK293, Vero E6 cells were grown in Dulbecco's modified Eagle's medium (DMEM, GIBCO) and HeLa cells were grown in Roswell Park Memorial Institute 1640 medium (GIBCO). HepG2 cells were grown in Minimum Essential Medium (MEM, GIBCO) supplemented with a 1% Nonessential Amino Acid Solution (NEAA, GIBCO). All media were supplemented with 10% heat-inactivated fetal bovine serum (GIBCO), 2 mM L-glutamine, 100 units/ml penicillin and 100 units/ml streptomycin, and cells were grown at 37°C under an atmosphere with 5% CO_2. Primary human umbilical vein endothelial cells (HUVECs) were grown in EGM-2 medium (Lonza) supplemented with 2% FBS, 0.04% hydrocortisone, 0.4% hEGF-B, 0.1% VEGF, 0.1% R3-IGF-1, 0.1% ascorbic acid, 0.1% hEGF, 0.1% GA-1000 and 0.1% heparin. Cells were treated with forskolin (FSK, Selleck), H89 (Selleck), 666-15 (MCE), KG-501 (Selleck), T-705 (Selleck), and lipopolysaccharide (LPS, Sigma) as noted in the text. Transient transfection was performed with Lipofectamine 3000 (Invitrogen) according to the manufacturer's instructions.

Mice

C57BL/6N AKIP1 knockout (*Akip1*$^{-/-}$) mice were generated by CRISPR-Cas9-mediated gene targeting by Cyagen Biosciences Inc., Suzhou. Briefly, Cas9 and AKIP1 gRNA targeting exon 4 (TGATCTGACTCCATCAGGCGAGG and ATACTACTTGTCTATGCCAGAGG) were coinjected into fertilized eggs. The *Akip1*$^{-/-}$ genotype was confirmed by PCR followed by sequence analysis using primers (Mouse *Akip1*-F: 5'- GTTCTCTCCCCAGCTTCTCAGTC -3'; Mouse *Akip1*-R: 5'- GCACCCATGTAGTTGAAAATAAAGC -3'), and 114 bp in exon 4 was demonstrated to be deleted. WT C57BL/6N mice (except littermates of *Akip1*$^{-/-}$ C57BL/6N mice) and BALB/c mice were purchased from Beijing Vital River Laboratory Animal Technology Co., Ltd. All mice were raised in the animal core facility at the Institute of Military Medical Sciences in accordance with the animal welfare requirements. 10 weeks old mice were used in the experiment otherwise indicated.

Vectors and viruses

Flag-tagged VP35, PRKACA (the catalytic subunit of PKA) and VP35 mutants were constructed by cloning the gene fragments into a pcDNA3.0-based Flag-vector (Invitrogen). Myc-tagged AKIP1 and mutants were constructed by inserting the gene fragments into the pCMV-Myc-vector (Clontech). GFP-tagged VP35 was expressed by cloning the genes into pEGFP-C1 (Clontech, Takara Bio). All the constructs were validated by Sanger DNA sequencing.

The small interfering RNA (siRNA) targeting AKIP1 (sense, 5'-GCAGUUGAU UCUGGACAAATT-3'; antisense, 5'-UUUGUCCAGAAUCAACUGCTT-3') (AKIP1 RNAi) and scrambled siRNA (sense, 5'-UUCUCCGAACGUGUCACGUTT -3'; antisense, 5'-ACGUGACACGUUCGGAGAATT-3') (si-control) were purchased from Genepharma Technologies (Suzhou, China). All siRNA transfections were performed using Lipofectamine 3000 (Invitrogen).

Recombinant adenoviruses (Type 5 adenoviruses with deletion of E1a and E3a genes) expressing VP35 (Ad-VP35) were obtained from Beijing BAC Biological Technologies. Analogous adenoviruses expressing GFP (Ad-GFP) or null (Ad-null) were used as controls. Live EBOV (Mayinga strain) is preserved by the BSL4 Lab in Wuhan Institute of Virology, Chinese Academy of Sciences.

Immunoprecipitation and immunoblot analysis

Cell lysates were prepared in lysis buffer containing 1% Nonidet P-40 and protease inhibitor cocktail (Roche)[42]. Soluble proteins were immunoprecipitated using anti-Flag (M2, Sigma), anti-Myc (Sigma), anti-VP35 (Creative Diagnostics), anti-CREB1 (Cell Signaling Technology) antibodies, or anti-mouse IgG antibody as a negative control (Sigma). An aliquot of the total lysate (5%, v/v) was included as a control. Immunoblotting was performed with horseradish peroxidase (HRP)-conjugated anti-Myc (Sigma), HRP-conjugated anti-Flag (Sigma), HRP-conjugated anti-β-actin (Sigma), anti-Phospho-(Ser/Thr) PKA substrate (Cell Signaling Technology), anti-VP35 (Creative Diagnostics), anti-L (Creative Diagnostics), anti-NP (Sino Biological), anti-AKIP1 (Abcam and Thermo), anti-pCREB1-133 (Abcam), anti-CREB1 (Abcam and Cell Signaling Technology), anti-c-Fos (Abcam), anti-phosphoserine (Abcam), anti-thrombomodulin (Abcam), anti-SerpinB2 (Abcam), or anti-PRKACA (BD). The antigen-antibody complexes were visualized via chemiluminescence (ECL system, GE Healthcare). A PageRuler Western marker (Thermo) was used as a molecular weight standard.

Purification of EBOV VP35 protein

EBOV VP35 proteins were expressed as His-tagged fusion proteins in *E. coli* BL21 (DE3) in Luria broth medium. EBOV VP35 protein expression was induced at an OD_{600} (optical density at 600 nm) of 0.6 with 0.2 mM isopropyl-D-thiogalactopyranoside (IPTG) and continued for 4 h at 37°C. Cells were then harvested and suspended in buffer (20 mM Tris and 8 M urea, pH 8.0). Suspended cells were sonicated and clarified by centrifugation at 12,000 rpm at 4°C for 15 min. Then, VP35-His protein was purified using a Ni column (Ni NTA beads 6FF), eluted with buffer (20 mM Tris, 8 M urea, and 500 mM imidazole, pH 8.0), and dialyzed to buffer (20 mM Tris-HCl and 300 mM NaCl, pH 8.0) for renaturation. The purity of the samples was determined by SDS-PAGE.

Quantitative RT-PCR

Total cellular RNA or viral RNA was extracted using the RNeasy mini (QIAgen, USA) or viral RNA mini (QIAgen, USA) according to the manufacturer's protocol respectively. For cDNA synthesis, 0.5 μg of RNA was reverse transcribed using ReverTra Ace qPCR RT master mix with gDNA remover (FSQ-301, Toyobo). The primer sequences are shown in Extended Data Table 1. The samples were denatured at 95°C for 2 min, followed by 40 cycles of amplification (15 s at 94°C for denaturation, 60 s at 60°C for annealing and extension). Quantitative RT-PCR was performed using SYBR Green Real-time PCR Master Mix (QPK-201, Toyobo) with the QuantStudio 6 Flex multicolor real-time PCR detection system (ABI). Relative mRNA levels to GAPDH were calculated using the $2^{-\Delta\Delta CT}$ method[43]. Means (upper limit of the box) ±SEM (error bar) of 3 independent experiments were presented in the figures.

In situ proximity ligation assay

The Duolink *in situ* proximity ligation assay (PLA) (Sigma) was used to detect the endogenous association of AKIP1 and VP35 in cells. In brief, HepG2 cells plated on glass coverslips were transfected with the plasmid expressing GFP-VP35. After fixation with 4% formaldehyde, cells were permeabilized with 0.3% Triton X-100 in PBS for 15 min. After blocking with blocking buffer, the cells were incubated with rabbit anti-AKIP1 (Abcam) or rabbit anti-GFP (Abcam) and mouse anti-VP35 (Creative Diagnostics) primary antibodies. anti-VP35 or anti-AKIP1 alone was employed as a negative control. Nuclei were stained with DAPI (blue). The red fluorescent spots generated from the DNA amplification-based reporter system combined with oligonucleotide-labeled secondary antibodies were detected with a Zeiss LSM 800 Meta confocal microscope (Carl Zeiss). Means (upper limit of the box) of the complexes number and ±SEM (error bar) from 10 cells were presented.

Immunofluorescence microscopy

Cells were transfected, fixed, permeabilized and blocked as described above. Then, after incubation with anti-AKIP1 (or other indicated primary antibodies) overnight at 4°C, the cells were washed three times with blocking solution and then incubated with FITC- or TRITC-conjugated goat anti-rabbit (or anti-mice) IgG. The cells were then stained with DAPI after washing, and imaged using a laser scanning confocal microscope (Zeiss LSM 800 Meta) with a 63× immersion oil lens. The intensity of CREB1 in the cytoplasm and the nucleus were analyzed by Image J.

Gene silencing using siRNA

For gene knockdown in HepG2 cells, cells maintained in 6-well plates were transfected with 100 pmol AKIP1 siRNA (sense, 5’- GCAGUUGAUUCUGGACAAATT -3’; antisense, 5’- UUUGUCCAGAAUCAACUGCTT -3’) or the same concentration of scrambled control siRNA (sense, 5’- UUCUCCGAACGUGUCACGUTT -3’; antisense, 5’- ACGUGACACGU UCGGAGAATT -3’) with Lipofectamine 3000 (Invitrogen) according to the manufacturer’s recommendations. For the minigenome assay, HEK293T cells were transfected with 100 pmol AKIP1 siRNA with Lipofectamine 3000. The minigenome assay was performed 24 h after siRNA transfection.

Generation of the AKIP1 knockout HepG2 cell line using CRISPR-Cas9 system

The *AKIP1* knockout cell lines were generated using the pSpCas9(BB)-2A-Puro (PX459) vector (Addgene plasmid no. 48139), with a single guide RNA (sgRNA) targeting the human *AKIP1* gene. The sgRNA sequences (target sequence 1: TGGCGGCCGCAGCGCTGAAT; target sequence 2: CATGTCTATCGTTATCA CAG) were designed using a CRISPR design web tool (http://crispr.mit.edu). The DNA sequences encoding sgRNAs were cloned into the CRISPR-Cas9 vector. Cells were transfected with the sgRNA vectors, and stable clones were screened by puromycin (1 μg/ml). Frameshift mutations in *AKIP1* gene were confirmed by sequencing and immunoblotting.

Luciferase reporter assay

Cells were seeded in 24-well plates and transfected with indicated amount of Flag-VP35, 200 ng of the CRE reporter plasmid (Promega, USA) and 4 ng of *Renilla* luciferase plasmid. An empty vector was used to ensure the same plasmid concentration in each well. After stimulation with or without 25 μM FSK for 4 h, the cells were harvested, and the luciferase activity of the cell lysates was analyzed with the dual-luciferase reporter assay system (Promega, USA) and measured in a TD-20/20 luminometer. Values were obtained by normalizing the luciferase values to the *Renilla* values. Fold induction was determined by setting the vector transfection without Flag-VP35 and without FSK as a value of 1.

PKA kinase activity assay

A PKA kinase activity kit was used (Enzo, USA) for the assay, which is based on a solid phase enzyme linked immunosorbent assay (ELISA) that utilizes a specific peptide as a substrate for PKA and a polyclonal antibody that recognizes the phosphorylated form of the substrate. Briefly, HepG2 cells were infected with Ad-VP35 or Ad-GFP at a MOI of 10. 48 h after infection, the cells were lysed, and the protein concentration was determined using the bicinchoninic acid (BCA) method. The PKA kinase activity in HepG2 cells was assayed according to the manufacturer's instructions. In brief, samples were added to wells of the PKA substrate microtiter plate. Then, diluted ATP was added to each well to initiate the reaction and incubated at 30°C for 90 min. Next, phosphospecific substrate antibody was added. After incubating at room temperature for 60 min, the diluted anti-rabbit IgG: HRP conjugate was added to each well and incubated at room temperature for 30 min. After washing, TMB substrate was added and incubated at room temperature for 30 min. Finally, stop solution was added, and the absorbance was measured at 450 nm. The relative kinase activity in cell lysate = (Average absorbance of sample-Average absorbance of blank) /Quantity of crude protein used per assay.

EBOV minigenome assay

The replication of EBOV in the cells was evaluated by the minigenome system[24]. Briefly, producer cells (p0) were co-transfected with p4cis-vRNA-RLuc (250 ng), pCAGGS-T7 (250 ng) expressing T7 RNA polymerase, and 4 plasmids expressing EBOV proteins (pCAGGS-NP (125 ng), pCAGGS-VP35 (125 ng), pCAGGS-VP30 (75 ng), and pCAGGS-L (1,000 ng)). One day after transfection, the medium was replaced with medium containing 5% FBS, and then incubated for another 3 days. Target cells (p1 or later) were transfected with pCAGGS-NP (125 ng), pCAGGS-VP35 (125 ng), pCAGGS-VP30 (75 ng), pCAGGS-L (1,000 ng) and pCAGGS-Tim (250 ng), incubated for 24 h, and then infected with replication and transcription-competent virus-like particles (trVLPs) from the p0 (or P1) supernatant for 24 h, and then cultured for another 3 days in medium containing 5% FBS. Virus replication was either determined by the intra-cellular luciferase activities using the Renilla-Glo luciferase assay kit (Promega, E2710) after cell lysis by passive lysis buffer (PLB; Promega), or by viral RNA level determined by reverse-transcription and quantitative real-time PCR.

Sucrose density gradient centrifugation

Sucrose gradient centrifugation was employed to fraction cell lysates as previously described[15]. WT and *AKIP1*$^{-/-}$ HepG2 cells grown in 100-mm dishes were transfected with plasmids expressing pCAGGS-NP (1.25 μg), pCAGGS-VP35 (1.25 μg), pCAGGS-VP30 (0.75 μg), pCAGGS-L (10 μg), pCAGGS-T7 (2.5 μg) and p4cis-vRNA-RLuc (2.5 μg). After 48 h, the cells were harvested and homogenized in 1 ml of lysis buffer (10 mM HEPES (pH 7.5), 12.5% sucrose, 1 mM EDTA, and 1× protease/phosphatase inhibitor cocktail) for 15 min at 4°C. The samples were then sequentially centrifuged at 700 and 1,000 × g for 5 min. Subsequently, the supernatants were layered onto continuous 25 to 60% sucrose gradients containing 10 mM HEPES (pH 7.5) and 1 mM $MgCl_2$ and then centrifuged at 137,000 × g for 2.5 h using an Optima MAX-XP (Beckman). Fractions were collected from top to bottom in 14-drop (300 μl) fractions. Then, the proteins in each fraction were subjected to immunoprecipitation and immunoblot analysis.

RNA immunoprecipitation (RNA-IP) assays

WT and *AKIP1*-depleted HepG2 cells were transfected with the plasmids pCAGGS-NP (1.25 μg), pCAGGS-VP35 (1.25 μg), pCAGGS-VP30 (0.75 μg), pCAGGS-L (10 μg), pCAGGS-T7 (2.5 μg) and p4cis-vRNA-RLuc (2.5 μg). After 48 h, the cells were lysed and assayed with the ChIP-IT High Sensitivity kit (53040, Active Motif, USA) as previously described. The CREB1 antibody (#9197, Cell Signaling Technology) was used to precipitate potential bound viral RNA. Precipitated RNA was reverse transcribed and quantified using real-time PCR. Primer pairs from EBOV 3' leader (3Le, 1-469) and 5' trailer (5Tr, 18283-18959) as described previously were employed[15]. The PCR primers are shown in Extended Data Table 1.

EBOV infection assay

WT or *AKIP1*-depleted HepG2 cells grown in 12-well plates were incubated with EBOV Mayinga strain, at a MOI of 1 for viral proliferation assay or a MOI of 10 for microscopy and qRT-PCR, at 37°C for 1 h. Then, fresh medium was added in the presence/absence of 10 μM H89 or 1 μM 666-15 and incubated at 37°C for 96 h. Subsequently, cells were fixed with 4% formaldehyde for immunofluorescence microscopy, or were lysed in 1 ml TRIzol reagent (Invitrogen) and viral RNA was extracted using a QIAamp viral RNA mini kit (QIAgen, USA) according to the manufacturer's protocol. EBOV RNA was quantitatively analyzed by reverse transcription and qRT-PCR. The viral titers were determined by plaque formation assay. Briefly, 10-fold serial diluted samples were added into a 96-well plate containing 1×10^4 Vero E6 cells per well. Cells were observed for cytopathic effect and the titers were expressed as median tissue culture infective dose ($TCID_{50}$). All work with live EBOV was performed in BSL4 containment.

mRNA expression microarray analysis

SurePrint G3 human gene expression 8x60k v2 microarray from Agilent was used for trancriptome analysis. Briefly, HepG2 cells were transfected with the plasmids Flag-VP35 or Flag. 48 h later, total RNA was extracted using the RNeasy mini kit (QIAgen, USA) according to the manufacturer's protocol. After first-strand cDNA synthesis with Poly-dT primer and second-strand cDNA synthesis, the cDNA was subjected to Gene Expression Microarray analysis following the manufacturer's protocol. The chips were

scanned with a GeneChip Scanner G2565CA (Agilent) and analyzed with Agilent Feature Extraction (v10.7) and GeneSpring software V13 (Agilent).

Tail bleeding time

Bleeding time was measured as previously described[44]. WT and *Akip1*$^{-/-}$ C57BL/6N mice (10 weeks, female) were infected with Ad-VP35 or Ad-null (2×10^9 PFU) via tail vein injection twice at 24 h intervals. Three days after the 2nd injection, WT mice were administered intraperitoneally with/without 2 mg/kg 666-15 (dissolved in 10% DMSO, 40% PEG300, 5% Tween-80 and 45% saline) three times at 24 h intervals. Six days later, the mice were challenged with LPS (5 mg/kg) or saline via their tail vein. After 4 h, the tails of the mice were cut transversely from the tip at 1 cm with surgical scissors. The bleeding tail stump was immediately placed in normal saline at 37°C, and the time was measured until the bleeding stopped.

Coagulation analysis

Mouse coagulation was measured as previously described with modifications[39]. WT and *Akip1*$^{-/-}$ mice were infected with Ad-VP35 or Ad-null (3×10^9 PFU) via tail vein injection twice at 24 h intervals. Six days later, the mice were injected with LPS (5 mg/kg) or saline via their tail vein. After 4 h, blood clotting times and serum FIB concentrations were determined using an automated blood coagulation analyzer (Rayto, RAC-030) according to the manufacturer's instructions.

Statistical analyses

Graphical representation and statistical analyses were performed using Prism 8 software (GraphPad Software). Unless otherwise stated, results are shown as mean (upper limit of the box) ±SEM (error bar) from 3 or more independent experiments in duplicate. Unpaired two-tailed *t*-test was used for the analysis of two groups. Survival curves were analyzed by Log-rank test. Data were considered significant when $p < 0.05$ (*), $p < 0.01$ (**), and $p < 0.001$ (***).

Reporting summary

Further information on research design is available in the Nature Research Reporting Summary linked to this paper.

Data availability

All data are available from the corresponding author upon reasonable request. Source data are provided with this paper.

Methods references

42 Cao, C., Leng, Y. & Kufe, D. Catalase activity is regulated by c-Abl and Arg in the oxidative stress response. *J. Biol. Chem.* **278**, 29667-29675 (2003).

43 Livak, K. J. & Schmittgen, T. D. Analysis of relative gene expression data using real-time quantitative PCR and the 2(-Delta Delta C(T)) Method. *Methods* **25**, 402-408 (2001).

44 Yang, P. *et al.* Antithrombotic Effects of Nur77 and Nor1 Are Mediated Through Upregulating Thrombomodulin Expression in Endothelial Cells. *Arterioscler. Thromb. Vasc. Biol.* **36**, 361-369 (2016).

Declarations

Acknowledgements

This work was supported by the National Natural Science Foundation of China [81590766] and National Major Science and Technology Projects of China [2018ZX09711003-005-005].

Author Contributions

G.X., X.L., and C.C. designed and supervised the study. L.Z., T.G., P.L., Y.J., Y.L., and H.L. performed the experiments. K.X., G.Z., L.Z., R.C., and W.Z. provided the EBOV minigenome system. Y.H., L.Z., and Y.W. performed the experiment related to EBOV infection in the BSL-4 laboratory. Y.H., W.Y., Q.D., G.W., T.Z., and D.W. analyzed the data. X.X. provided experimental guidance. L.Z, X.L., and C.C. wrote the manuscript.

Competing Interests statement

The authors declare no competing interests.

Figures

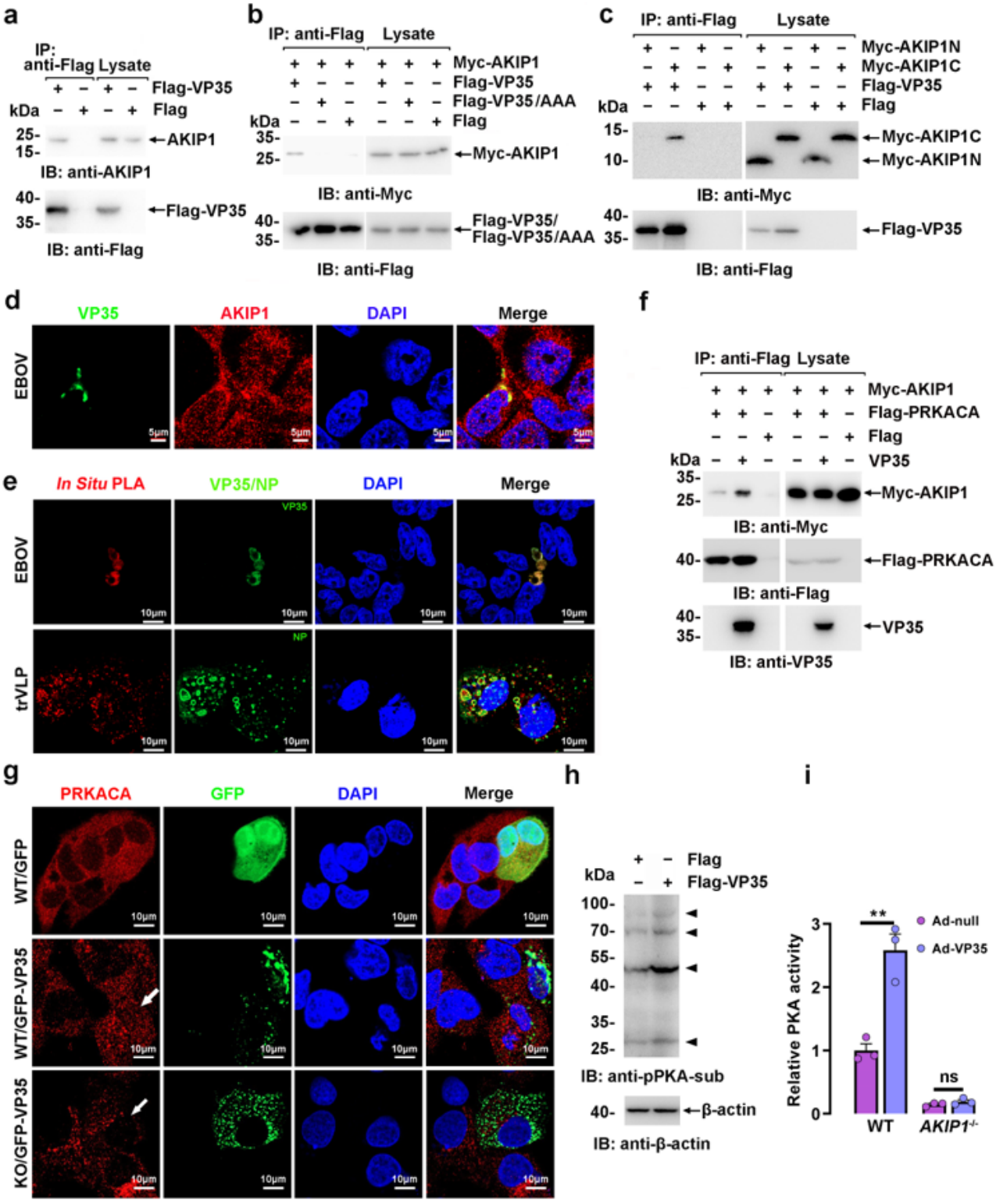

Figure 1

The EBOV VP35 associates with AKIP1 and activates PKA. a-c, Lysates of HepG2 cells (a) or HEK293 cells (b, c) expressing indicated plasmids were subjected to anti-Flag immunoprecipitation and analyzed by immunoblotting. d, HepG2 cells infected by Zaire EBOV (strain Mayinga) (MOI=10) for 48 h were analyzed by immunostaining with anti-VP35 (green) and anti-AKIP1 (red) antibodies. e, HepG2 cells infected with live EBOV or transfected with EBOV minigenome (p0) were subjected to in situ PLA assay

with anti-VP35 and anti-AKIP1 antibodies, and immunostaining with an anti-VP35 (green) (upper panel) or anti-NP (green) (lower panel) antibody. f, Lysates of HEK293 cells co-transfected with indicated plasmids were incubated with/without recombinant His-VP35 for 2 h, and then subjected to immunoprecipitation and immunoblotting analysis. g, Wild-type (WT) and AKIP1 knockout (KO) HepG2 cells transfected with GFP-VP35 or GFP were treated with FSK (25μM) for 45 min, and were subjected to anti-PRKACA immunostaining (red). Arrow: Cells expressing GFP-VP35. h, Lysates of HepG2 cells transfected with indicated plasmids were analyzed by immunoblotting. i, Lysates of WT and AKIP1 KO HepG2 cells infected with Ad-VP35 or Ad-null (MOI=10) were subjected to PKA activity assay. PKA activity values of three independent replicates (n=3) were normalized and expressed as mean +-SEM (**P<0.01).

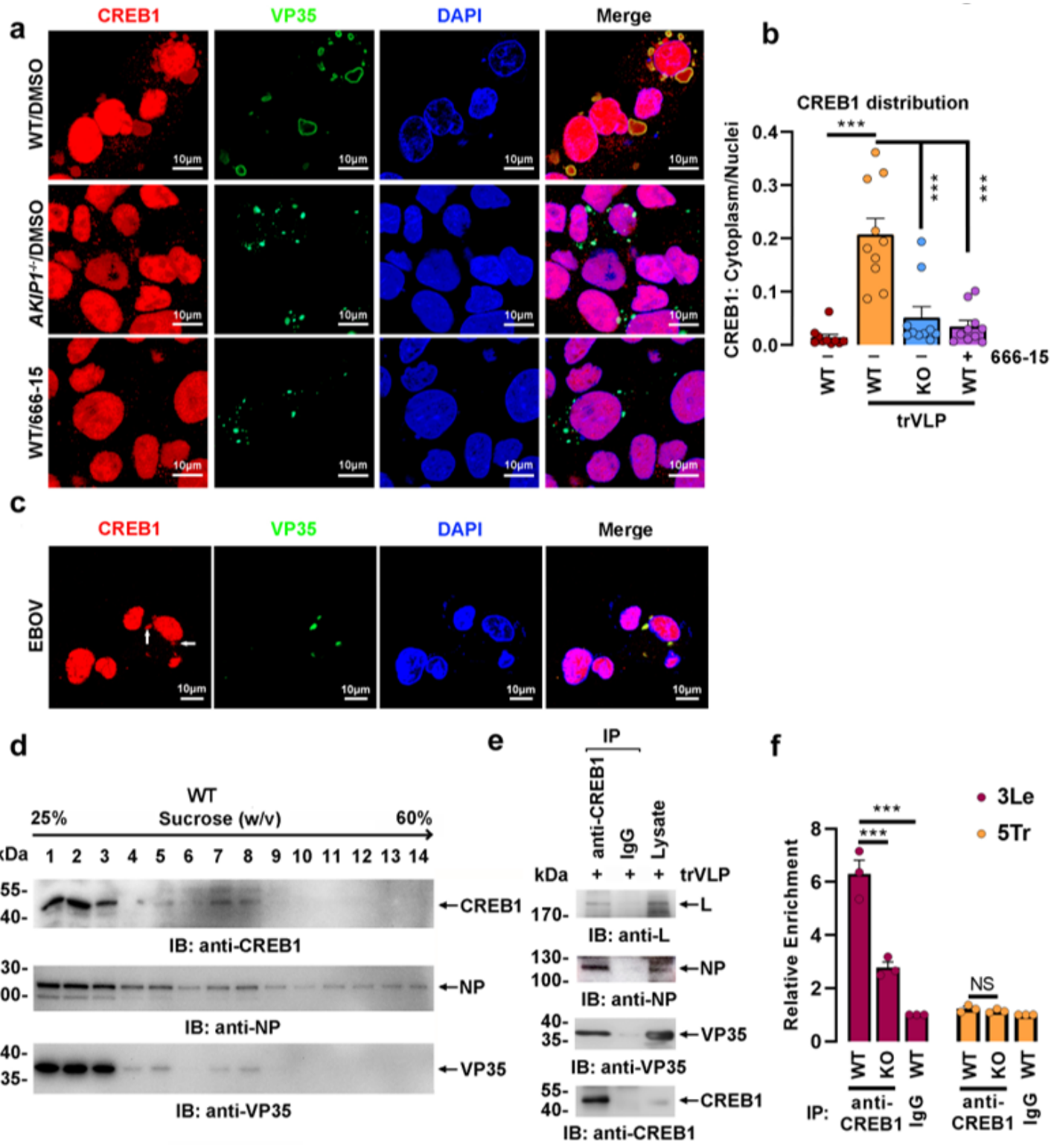

Figure 2

EBOV VP35 promotes CREB1 phosphorylation at S133 in vitro and in vivo via AKIP1. a, HepG2 cells infected with Ad-VP35 or Ad-GFP for 48 h were treated with 25 μM FSK or 10 μM H89 for 4 h, and then analyzed by immunoblotting. b, HepG2 cells expressing GFP-VP35 or GFP were subjected to immunostaining with an anti-pCREB1(S133) antibody (red). c, HepG2 cells infected with live EBOV (upper panel) or transfected with EBOV minigenome (p0) (lower panel) were subjected to immunostaining with

indicated antibodies. d, HepG2 cells transfected with AKIP1 RNAi or scrambled siRNA were infected with Ad-VP35 or Ad-GFP for 36 h. Then, lysates were analyzed by immunoblotting. e, Lysates of WT and AKIP1 KO (two independent clones) HepG2 cells infected with Ad-VP35 or Ad-GFP were analyzed by immunoblotting. f, C57BL/6N mice were intravenously injected with Ad-VP35 or Ad-null (2×109 PFU) twice at an interval of 24 h. Three days post the first infection, the liver tissues (upper panel) and lung (lower panel) tissues were analyzed by immunohistochemistry staining with an anti-pCREB1(S133) antibody.

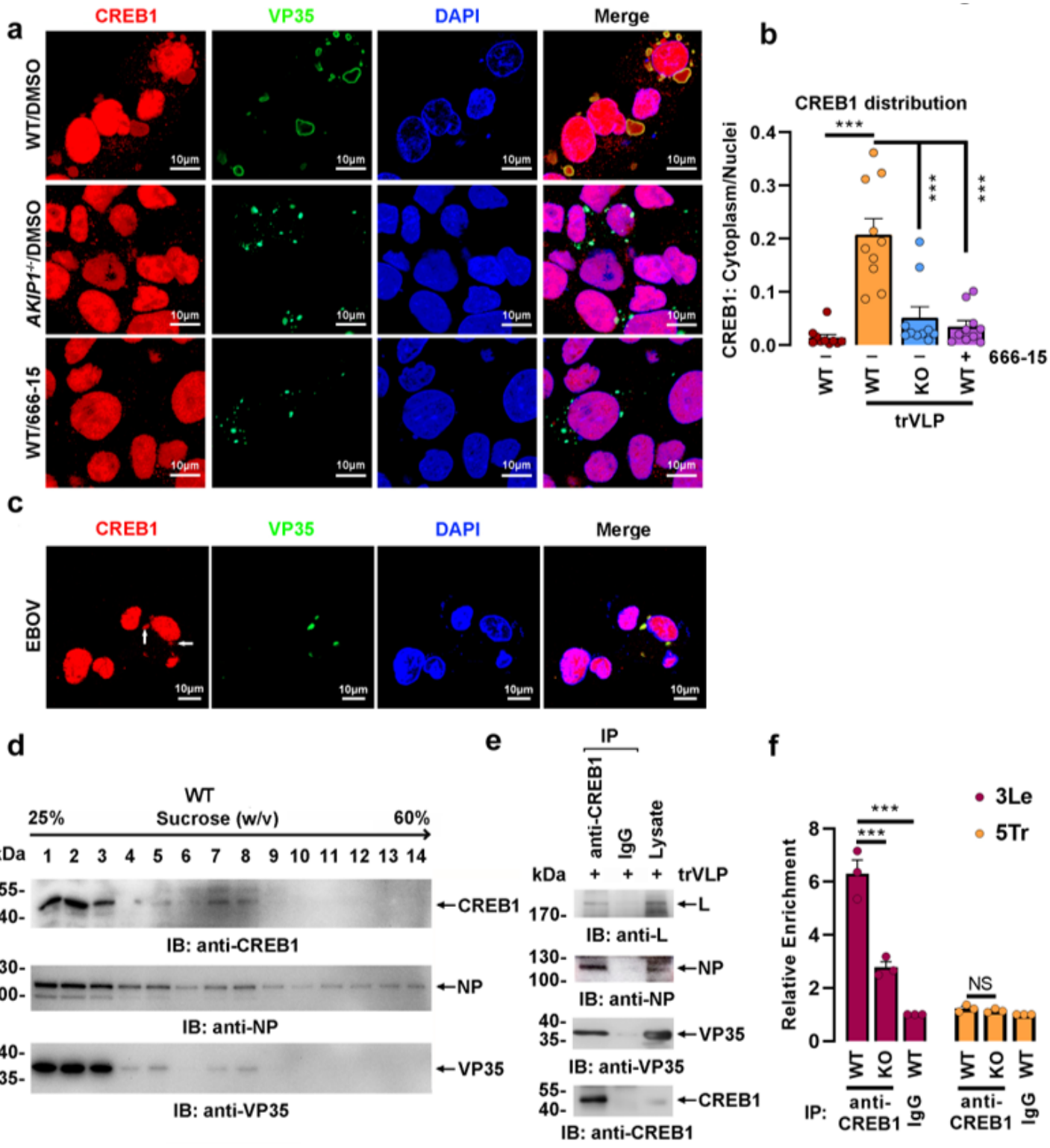

Figure 3

CREB1 is recruited to viral inclusion bodies upon trVLPs or EBOV infection. a, b, WT and AKIP1 KO HepG2 cells were transfected with EBOV minigenome (p0) with or without 1 μM 666-15 treatment for 48 h and then immunostained with anti-VP35 (green) and anti-CREB1 (red) antibodies (a). Cytoplasm/nuclei distribution of CREB1 in (a) was analyzed by ImageJ software (b). The ratio of CREB1 distribution in at least 10 cells was expressed as mean +-SEM (***P<0.001). c, HepG2 cells infected with live EBOV were immunostained with anti-CREB1 (red) and anti-VP35 (green) antibodies. d, Lysates of HepG2 cells transfected with EBOV minigenome (p0) were separated on a 25 to 60% (W/V) sucrose gradient. Fractions were collected and analyzed by immunoblotting. e, The 7th and 8th fractions from (d) were combined and subjected to immunoprecipitation and immunoblotting analysis. f, WT and AKIP1 KO HepG2 cells were transfected with EBOV minigenome (p0). Cell lysates were subjected to anti-CREB1 (or IgG as control) immunoprecipitation, and the co-precipitated viral RNA corresponding to 3Le or 5Tr was quantified by qRT-PCR. Mean +-SEM from 3 independent assays were presented (***P<0.001).

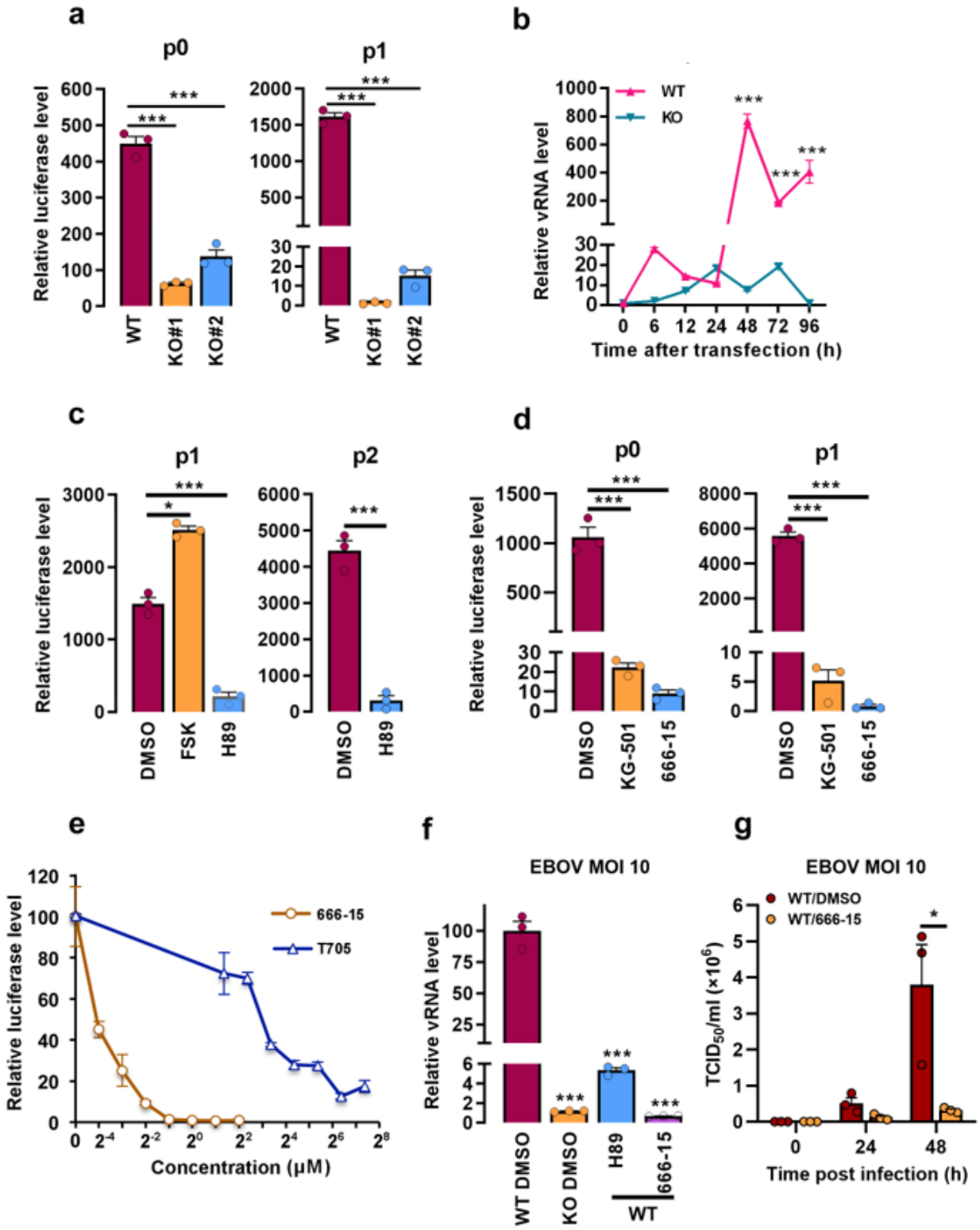

Figure 4

AKIP1-PKA-CREB1 potentiates trVLPs and EBOV replication. a, b, WT and AKIP1 KO HepG2 cells were transfected with EBOV minigenome (p0 and p1) for 96 h. Cells were lysed and the amounts of trVLPs in the cells were determined by luciferase activity assay (a). vRNA was quantified at indicated time-points by qRT-PCR (b). c, d, HEK293 (c) or HepG2 (d) cells were transfected with EBOV minigenome (p0, p1 and p2) and treated with FSK (25 μM) or H89 (10 μM) for 4 h (c), or CREB1 inhibitors (1 μM 666-15 or 25 μM

KG-501) for 48 h (d). The amounts of trVLPs were determined by luciferase activity assay. e, HepG2 cells were transfected with EBOV minigenome (p0 and p1) for 24 h. Then, p1 cells were treated by 666-15 or T-705 at indicated concentrations for 24 h. The amount of trVLPs was determined by luciferase activity assay and normalized by DMSO treatment group (set as a value of 100). f, g, WT and AKIP1 KO HepG2 cells infected with live EBOV were treated with 10 μM H89 or 1 μM 666-15 for 96 h. vRNA level in the cells was quantified by qRT-PCR (f). Meanwhile, the cell culture supernatants were collected at indicated time-points, and the viral titers were quantified as TCID50 with plaque assay (g). All data of 3 independent experiments were expressed as mean +-SEM except (e) as mean +-SD (*P<0.05; ***P<0.001).

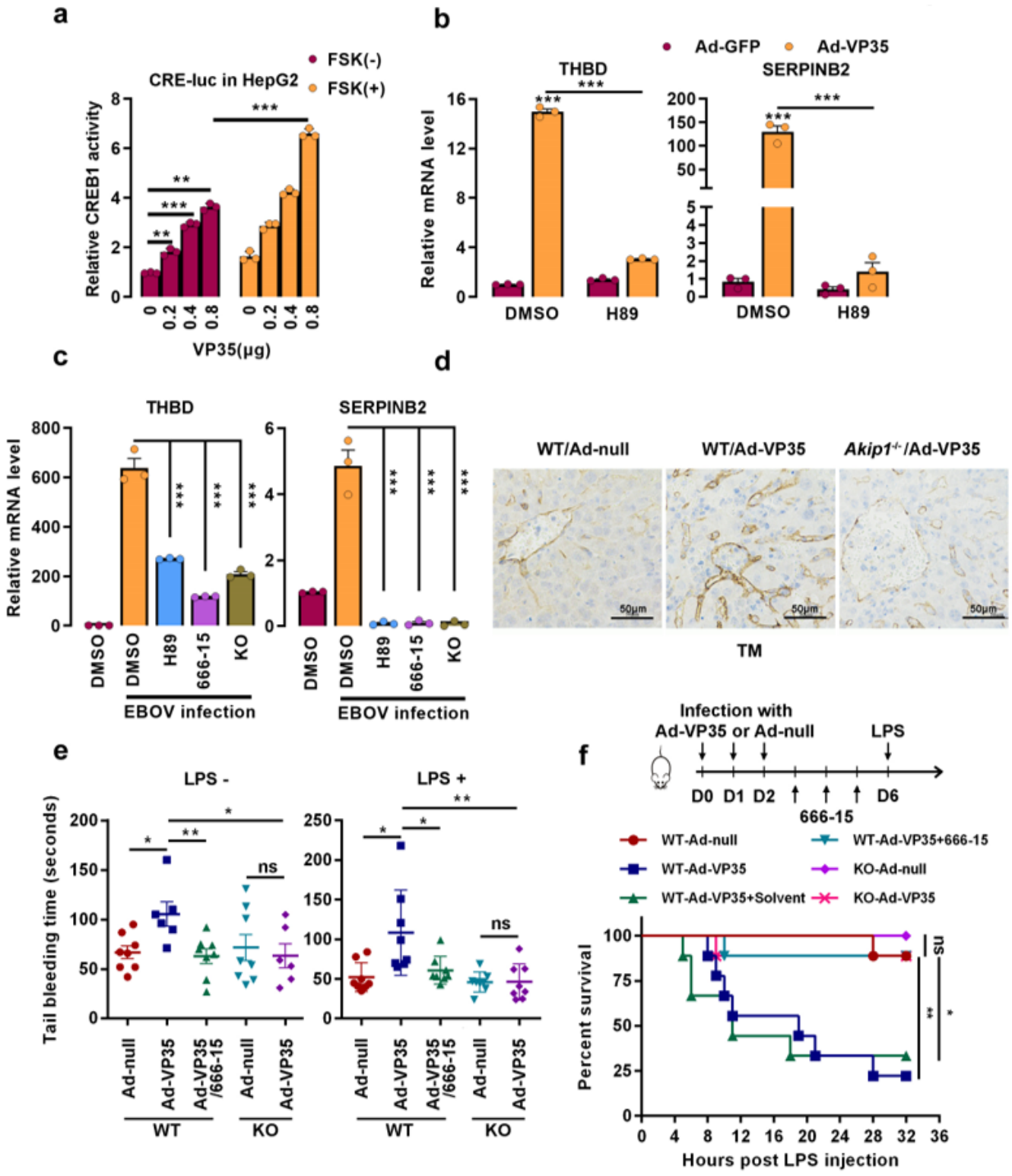

Figure 5

EBOV VP35 promotes the transcription of CREB1-directed coagulation-related genes. a, HepG2 cells co-transfected with pGL-CRE-Luc, pRL-TK and indicated amounts of Flag-VP35 were treated with or without 25 μM FSK for 4 h. The luciferase activity of the cell lysates was analyzed. b, c, HUVECs (b), WT or AKIP1 KO HepG2 (c) cells infected with Ad-VP35 (b), or live EBOV (c) for 48 h were treated with or without 10 μM H89 or 1 μM 666-15 for another 24 h. THBD and SERPINB2 mRNA levels were determined by qRT-PCR. d,

WT or Akip1 KO mice were intravenously injected with Ad-VP35 or Ad-null (2×109 PFU) twice at an interval of 24 h. Six days post the first infection, the liver tissues were analyzed by immunohistochemistry staining with an anti-TM antibody. e, f, Mice were infected with Ad-VP35 or Ad-null, treated with 666-15 (2 mg/kg) or solvent, and then challenged with or without LPS. The tail bleeding time was determined (n=8) (e) and mice survival curve was demonstrated in f (n=9). All data of 3 independent experiments were presented as the mean ±SEM (*P<0.05; **P<0.01; ***P<0.001).

Supplementary Files

This is a list of supplementary files associated with this preprint. Click to download.

- ExtendedData.docx